Korean J. Chem. Eng., 36(5), 763-779 (2019)
DOI: 10.1007/s11814-019-0251-9

pISSN: 0256-1115
eISSN: 1975-7220

CO_2 separation over light gases for nano-composite membrane comprising modified polyurethane with SiO_2 nanoparticles

Mohammdad Hadi Nematollahi*,‡, Shahryar Babaei,‡, and Reza Abedini***,†**

*CICECO - Aveiro Institute of Materials, Department of Chemistry, University of Aveiro, 3810-193 Aveiro, Portugal
**Department of Chemical Engineering, Faculty of Engineering, Shiraz Branch, Islamic Azad University, Shiraz 7473171987, Iran
***Faculty of Chemical Engineering, Babol Noshirvani University of Technology, Babol 4714871167, Iran
(*Received 22 December 2018 • accepted 3 March 2019*)

Abstract–Owing to the potential of polymeric and nanocomposite membranes for industrial application in CO_2 capturing and gas separation processes, permeation properties of CO_2, N_2 and O_2 through the polymer matrix have been an object of extensive research. We measured the permeation rates of gases (pure and mixed gas) within a novel nanocomposite membrane composed of poly tetramethyleneglycol (PTMG), hexamethylene diisocyanate (HDI), and diamine chain extender, 4,4-methylenebis(2-chloroaniline) (MOCA) at various silica loadings and operating conditions. The novel polyurethane was prepared by a two-step bulk polymerization technique based on the molar ratios of the used constituents 1 : 3 : 2 for PTMG : HDI : MOCA, respectively. The FTIR spectra indicated that the extent of phase separation decreased by increase in the SiO_2 content. From the DSC and XRD analyses, the existence of small crystalline areas within the soft and hard segments of matrix was proved. High thermal stability of new nanocomposites was authenticated by a 90 °C increase in the decomposition temperature upon including the SiO_2 particles into the polymer matrix. By providing a longer diffusion path, a reduction in the permeation of penetrants occurred after the incorporation of SiO_2 content. By raising the temperature from 25 to 45 °C, the gas permeation value of CO_2, O_2 and N_2 rose steeply: 35, 54 and 81% in neat PU and 49, 64 and 137% in PU containing 15 wt%, respectively. Conversely, the obtained results for increasing the feed gas pressure from 6 to 10 bar revealed that the penetration of non-condensable gases, O_2 and N_2, decreased while the permeation rate of CO_2 polar gas surged dramatically. Nevertheless, a simultaneous increment in the selectivity amounts of both gas pairs was revealed. For the gaseous mixtures, the trend of changes in permeability and selectivity values were almost identical with those of pure gas: decrease in permeation, and vice versa increase in gas pair selectivity. Eventually, the separation results of the prepared membranes indicated a strong tendency to move towards Robeson's line by incorporation of SiO_2 nanoparticles into the matrix of membranes.

Keywords: Polyurethane, Nanocomposite, PTMG, MOCA, SiO_2, Gas Separation

INTRODUCTION

Global warming is mainly the result of CO_2 levels rising in the Earth's atmosphere, and both atmospheric CO_2 and climate change are accelerating [1]. Climate scientists say we have years, not decades, to stabilize CO_2 and other greenhouse gases. As a consequence, the earth's climate is changing in such a way that Surface temperatures in the 21st century have been notably higher than temperatures in the middle and late 20th century. According to a 2015 report, BP released its annual energy outlook predicting a 37% increase in global demand for energy; as a result, carbon dioxide emissions would likely rise by 25% by 2035. Distinctively, due to the global greenhouse gas (GHG) emissions, the exceeding trend of global warming has been directed into various problems and proper solutions should be taken. Meanwhile, membrane separation processes, due to their potential energy saving capacity, lower operating and maintenance cost, ease of processing and also the least impact on the environment, have become one of the emerging technologies which have undergone a massive growth during the past few decades [2-4]. It is crystal clear that separation is fulfilled due to differences in the diffusion rates of feed constituent elements; therefore the high permeation rate of each gas is the underlying cause of utilizing membrane for industrial applications. Moreover, gas pair selectivity is another key factor for separation. Clearly, ideal selectivity owing to economic appraisal is of the utmost importance but increase in permeability leads to decrease of selectivity. Thus, establishing a delicate balance between them would result in a desired separation, particularly for commercial purposes.

A major question that often arises with the application of materials is how to find the most promising structures for a given application in the diverse pool of existing materials. In this regard, rubbery polymers and some glassy types with high free volume have been extensively applied to exploit the potential of their high permeability, which simultaneously expresses fairly acceptable selectivity values. Given the results of other researchers, glassy polymers have revealed tremendous values of permeance. Among those, substituted polyacetylenes [5-8], perfluoropolymers [9,10], addition-type polynorbornene [11,12] and polymers of intrinsic microporosity

†To whom correspondence should be addressed.
E-mail: abedini@nit.ac.ir
‡M. H. Nematollahi (m.nematollahi@ua.pt) and S. Babaei contributed equally to this work.

(PIMs) [13-16] have vividly shown prodigious degrees of permeability; however some of them, such as poly(4-methyl-1-pentene) (TPX) [3,17,18] and few PIMS, have presented a fine-tuned performance. Under this circumstance, there has been an increasing tendency for investigators and research groups to scrutinize thoroughly rubbery polymers which exhibit high permeation rate as well as adequate selectivity for gas pairs [19-23] along with high chain mobility, superior thermal stability and entirely compatible for blending with other polymers.

Among rubbery polymers, polyurethanes (PU) are one of a distinguished species of polymers that have profoundly shifted all the attention to themselves because of their excellent physical and thermomechanical properties, considerable degree of elasticity, high tensile strength, tolerable dimensional stability, good chemical resistance, relatively good biocompatibility, wide applicability [24,25] and moderate permselectivity [26,27]. By the virtue of their tailorable properties, PUs have expressed a rich diversity of applications such as coatings, adhesives, sealants, foams (flexible or rigid), paints, varnishes, leathers, rubbers, fibers, films, biomimetic materials and many more [28,29]. In addition, the expansive applicability of PU coatings is assigned to versatility in selection of monomeric substances from a comprehensive list of macrodiols, diisocyanates and chain extender. Nonetheless, its unique properties can be enormously reinforced by incorporating nanoparticles into PU matrix or blending with other polymer, whether glassy or rubbery. Thus, the possibility of fabricating the novel materials with high potential for new applications would be easily achievable upon the addition of nanoparticles into polymer structure. The inclusion of inorganic nanoparticles into organic polymers leads to change in the polymer structure [30], which enhances permeation of gases, in particular smaller molecules like CO_2. In addition, change in physical features such as thermal, mechanical, dielectric and magnetic properties [24,31-33] is another extraordinary influence of nanoscale particles on polymeric membranes in such a way that boosts their performance substantially.

A large number of gas transport properties of PU nanocomposite membranes have been studied in the literature. Recently, Afarani et al. examined the optimization of operating parameters including pressure, temperature and filler content that influenced on the gases' permeation rate through PU-zeolite hybrid membranes using the response surface method software [34]. The influence of embedded MWCNTs particles into PU membrane for CO_2/CH_4 separation was examined to improve the performance of fabricated nanocomposite membranes. MWCNTs were functionalized with tetraethylene pentamine (TEPA) and then incorporated into polymer structure. The results indicated that the permeation rate of CO_2 experiences a dramatic enhancement from 198.4 to 396.5 barrer at 10 wt% of filler content. Surprisingly, it was two-times more than the pure PU sample. Nonetheless, they reported just 9.6% increase for CO_2/CH_4 selectivity [35]. Karimi and Hassanajlili studied gas separation properties by short fiber/PU composite membrane. To do this, short glass wool fiber (SGWF) was applied as a polar micro size reinforcement. Their results detected a simultaneous increment in CO_2 permeability and CO_2/CH_4 selectivity values. For example, just by incorporation of 1 wt% of SGWF into PU matrix, the permeability of CO_2 and CO_2/CH_4 selectivity significantly rose from 27.88 to 34.8 barrer and 7.20 to 13.19, respectively [36].

Sadeghi et al. investigated the gas permeation properties of a polycaprolactone composite membrane including 1,4-butandiol (BDO) as chain extender. The gas permeability of membranes decreased as the amount of silica nanoparticles increased, while the selectivity of CO_2/N_2, CO_2/CH_4 and O_2/N_2 gas pairs went up markedly [37]. As the chain extender can change the properties of hard segment of PU matrix and subsequently affect the bandings between soft and hard segments, a new diamine extender was substituted in the structure of PU. Diamine chain extenders are able to establish a stronger hydrogen bonding than diol extenders, and thus the separation properties would change. On the other hand, silica nanoparticles are highly promising for industrial applications owing to their excellent compatibility, thermal stability, facile synthetic route, large-scale synthetic availability, and more importantly revealing strong tendency toward CO_2 due to its - OH group in its structure. The particle size, crystallinity, porosity, and shape can be precisely manipulated, enabling the silica nanoparticles for various applications. Therefore, here, a novel nanocomposite membrane by MOCA chain extender and embedding an inorganic nanoparticle in the structure of PU were fabricated to find the MOCA effects on membrane permselectivity.

The gas transport properties of fabricated nanocomposite membranes were appraised via pure CO_2, O_2 and N_2 and also CO_2/N_2 and O_2/N_2 mixed gas permeation. Further, the impacts of increasing the filler content and operating conditions (e.g., temperature and pressure) on each gas permeability and gas pairs selectivity were analyzed in great depth aiming to give guidance for selection suitable polymers for efficient gas separation/capture. Finally, the permeation behavior of the PU nanocomposite membranes was compered to Robeson's upper bound limit.

MATERIALS AND METHODES

1. Materials

Table 1 illustrates the constituents of urethane, applied gases, sol-

Table 1. Description of chemical materials used in this work

Chemical name	Chemical formula	CAS	Abbreviation	Purity	Supplier
Polytetramethylene glycol	$(C_4\text{-}H_8\text{-}O)n\text{-}H_2\text{-}O$	25190-06-1	PTMG	≥98	APC, Iran
hexamethylene diisocyanate	$C_8H_{12}N_2O_2$	822-06-0	HDI	≥98	Merck, Germany
4,4-methylene-bis(2-chloroaniline)	$C_{13}H_{12}Cl_2N_2$	101-14-4	MOCA	≥98	Aldrich, USA
Dibutyltin dilaurate	$C_{32}H_{64}O_4Sn$	77-58-7	DBTDL	95	Merck, Germany
N-Methyl-pyrrolidone	C_5H_9NO	872-50-4	NMP	≥99	Merck, Germany
Silicon dioxide (Silica)	SiO_2	7631-86-9	SiO_2	99.5	Tecknon, Spain

vents and nanoparticle that were used. Polytetramethylene glycol (PTMG, M_w=2,000 g·mol^{-1}) was placed in a vacuum oven for 24 h at 85 °C in order for the process of removing the residual water. However, diisocyanates were used without any pretreatment. Dibutyltin dilaurate (DBTDL) and N-Methyl-2-pyrrolidone (NMP) were used as a catalyst to advance the process of polyurethane synthesis and PU solvent, respectively. Silica (SiO_2) nanoparticles, manufactured by Tecknon Company, were used as an inorganic additive. The additional specifications and sources of the chemicals used in this work are summarized in Table 1.

2. Polyurethane Synthesis Reaction

Polyurethanes included PTMG/HDI/MOCA (polyol/DI/chain extender). For PU sample synthesis, a two-step bulk polymerization method was applied. In the first step, PTMG and HDI were added to the reaction container and the reaction continued until HDI was exhausted. In this step, a pre-polymer with high molecular weight was ready. Due to a deep deficiency in mechanical properties, the pre-polymer was sent to the second step in which the prepared pre-polymer with the chain extender entered the reaction container. In this stage with extending the chain, the PU with desirable properties was fabricated.

Regarding bringing the reaction to completion, DBTDL catalyst was added to the mixture of PTMG and HDI. The mixture was incubated for 3 h at 85-90 °C under nitrogen atmosphere to form a macrodiisocyanate pre-polymer. Then, the chain extension of the pre-polymer was carried out by addition of MOCA at room temperature for 5 minutes. The prepared polymer was taken from the container and placed in the oven for 24 h at 95 °C to obtain complete reaction. To attain a linear polymer, the molar ratio of NCO : NH_2 was kept at 1 : 1. Furthermore, the molar ratios of the used constituents, PTMG : HDI : MOCA, were 1 : 3 : 2, respectively. The two-step reaction technique of polyurethane synthesis and molecular structure of PU-urea is shown in Fig. 1. As can be seen, the presence of MOCA diamine chain extender leads to urea linkages.

Table 2. Solution composition of synthesized membranes

Membrane	Polymer (10 wt%)		Solvent (wt%)
	PU	SiO_2	NMP
PETU	100	0	90
PETU5	95	5	90
PETU10	90	10	90
PETU15	85	15	90

3. Preparation of Membranes

Neat membrane was fabricated via solution casting method by dissolving 10 wt% of PU in NMP and stirring for 2 h at 80 °C. After filtering, the prepared solution was cast in a Teflon glass petri dish and heated in a convection oven for 24 h at 80 °C. Then, to prepare a largely homogeneous membrane, it was placed in a vacuum oven at 80 °C for another 3 h to remove residual solvent. For nanocomposite membranes, the membrane preparation process was exactly analogous to pure PU with the previous step of silica distribution in NMP solvent. To obtain uniform dispersion of particles, the SiO_2 solution was exposed to ultrasonic waves for 50 min. Next, PU was added to the solution and stirred for 2 h at 80 °C. In subsequent steps, the mixture was again placed in an ultrasonic bath for another 10 min. After casting, it was left for 24 h at 80 °C in an oven and also 3 h at 80 °C under vacuum condition. Eventually, the thickness of the synthesized membranes was measured around 100 μm using a micrometer caliper. Table 2 presents the all membranes prepared via casting solution with corresponding codes.

4. Characterization

4-1. FTIR Spectroscopy

To indicate the distinctive features of the prepared polyurethane membranes, such as the chemical structure of PU and the level of polar groups as well as the created bonds, a 27 Tensor FTIR spec-

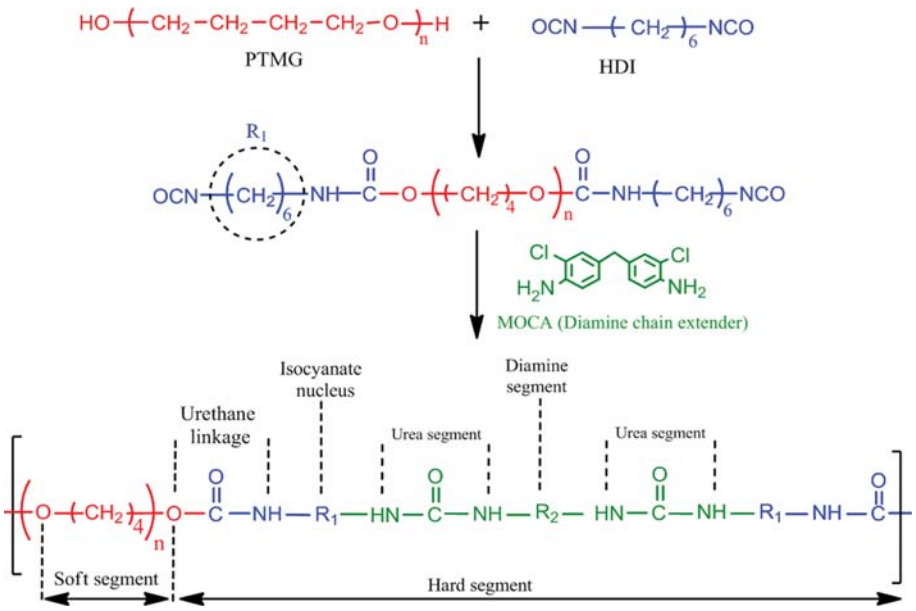

Fig. 1. Molecular structure of the fabricated polyurethane.

trometer (ATR, Bruker) was utilized. The range of scanning frequency was 4,000-600 cm^{-1}.

4-2. Scanning Electron Microscopy (SEM)

To probe exactly the morphological features of the fabricated membranes in the presence of silica contents and also the accumulation and distribution of silica particles within the PU matrix, scanning electron microscopy (SEM) (KYKY-EM 3200) was used.

4-3. Thermal Analysis

Thermal behavior of synthesized membranes was appraised by differential scanning calorimetry analysis (DSC) (Mettler Toledo, DSC822e) through double scanning at heating rate of 10 °C·min^{-1} and the temperature range of 100-200 °C. Thermal stability and degradation temperature of all synthesized membranes were accurately assessed by thermal gravimetric analysis (TGA, Mettler Toledo). To carry out TGA analysis, a 17 mg of each sample was placed in a platinum pan and heated to 600 °C (20-600 °C) with a heating rate of 10 °C/min under nitrogen flow.

4-4. XRD Analysis

The crystal structure of prepared membranes was inspected by X-ray diffractometer manufactured by Philips, Netherlands (XRD, PW 3040). The obtained patterns were recorded by monitoring the diffraction angle 2θ from 10-60° at a scan rate of 0.01°/min using copper radiation under a voltage of 40 kV and a current of 40 mA.

5. Gas Permeability Measurements

To measure the gas transport properties of prepared membranes, a constant pressure/variable volume set-up system was used. The typical membrane area placed in the module was 10.75 cm^2. The pressure of input stream (pure CO_2, O_2 and N_2 gases and mixed gases of CO_2/N_2 and O_2/N_2 with 50 : 50 v/v) was 6, 8 and 10 bar, while the permeate side was kept at atmospheric pressure. Moreover, the temperature of feed gas increased from 25 to 45 °C. The right quantity of the permeance of gases was determined by mass flow meter and the corresponding gas permeability was computed by the following equation:

$$P = \frac{QL}{(P_1 - P_2)A} \tag{1}$$

where P is the permeability expressed in barrer (1 barrer=10^{-10} cm^3 (STP)·cm·cm^{-2}·s^{-1}·$cmHg^{-1}$), Q is flow rate of the permeate gas passing through the membrane (cm^3/s), L is membrane thickness (cm), P_1 and P_2 are the absolute pressures of the feed and permeate sides (cmHg), respectively, and A is the membrane effective area (cm^2). In addition, the ideal permselectivity of A gas than B gas ($\alpha_{A/B}$) was counted by dividing the gas permeation as follows:

$$\alpha_{A/B} = \frac{P_A}{P_B} \tag{2}$$

The gas mixture selectivity was measured by the following equation:

$$\alpha_{A/B} = \frac{y_A/y_B}{x_A/x_B} \tag{3}$$

where y and x are the volumetric fractions of the permeate and

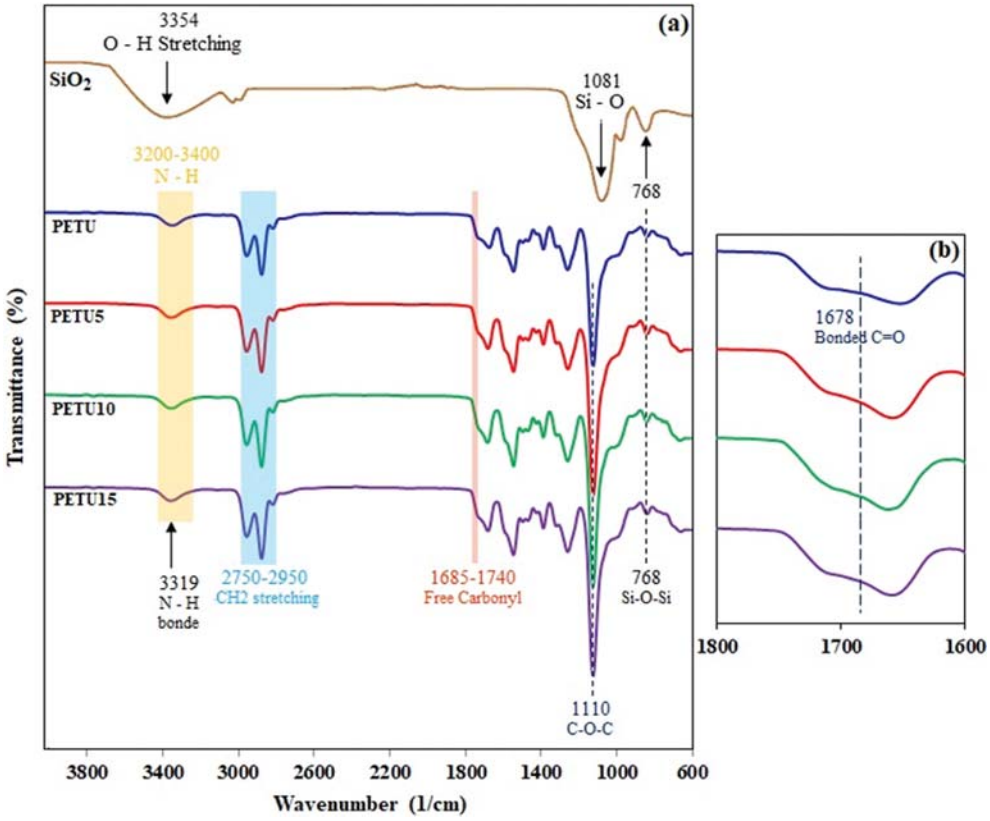

Fig. 2. (a) ATR-FTIR spectra of PU impregnated with silica nanoparticles, (b) absorption region of carbonyl groups synthesized polyurethane membranes.

feed gas, respectively. The permeate gas was analyzed by means of a gas chromatography apparatus (GC model ACME 6100 Young Lin Instrument Co., Korea) equipped with a thermal conductivity detector (TCD) and a Q capillary column was used for permeate analysis. The carrier gas was also Helium.

RESULTS AND DISCUSSION

1. Membrane Characterization

1-1. FTIR Analysis

Figs. 2(a) and (b) illustrate FT-IR spectra of all fabricated membranes with the effect of SiO_2 loading on the membrane structure. The formed bonds and all functional groups are exhaustively analyzed in Fig. 2(a). Moreover, the absorption results of the carbonyl groups (C=O bond) to fully comprehend the phase separation phenomenon are in Fig. 2(b).

Regarding the FT-IR spectra of SiO_2 shown in Fig. 2(a), there is a wide region between 750-1,260 cm^{-1} which can be portrayed as a superimposition of assorted SiO_2 peaks, Si-OH bonding and peaks due to residual organic groups. Clearly, the two absorption bands at 768 and 1,081 cm^{-1} are the strongest peaks assigned to symmetric and asymmetric vibration of Si-O, respectively. Another peak arising from asymmetric vibration of Si-OH is revealed at 979 cm^{-1}. Furthermore, the impact of water content strongly emerges in 3,200-3,500 cm^{-1} attributed to O-H stretching in H-bonded water The absorption band at 2,932 cm^{-1} (CH_2) and 2,981 cm^{-1} (CH_3) can be asscribed to the presence of unreacted TEOS in the silica particles [38].

From Fig. 2(a), the FTIR result of neat PU discloses that the equivalent wave of NCO bond at 2,270 cm^{-1}, due to the complete reaction of isocyanates groups, would be vanished. As can be clearly seen, the band intensity in the NH includes a broad region in 3,200-3,400 cm^{-1}. The absorption peak at approximately 3,319 cm^{-1} reveals the most intensive band ascribed to the N-H stretching vibrations in hydrogen bond to carbonyl group (hard-hard segment interactions). Furthermore, upon inclusion of silica content into PU matrix, an additional band at around 3,275 cm^{-1} can be detected. This directly corresponds to the N-H stretching vibrations hydrogen bonded to either oxygen (hard-soft segment interactions) [39]. Although the urethane-bonded carbonyl group occurs at around 1,678 cm^{-1}, the waves arising from 1,685-1,740 cm^{-1} show symptoms of free carbonyl groups. The sharp peak at 1,110 cm^{-1} is assigned to the anti-symmetric stretching vibrations of the non-associated ether C-O-C in PETU soft segments. The wave numbers between 2,750-2,950 cm^{-1} show signs of -CH_2 stretching bond [40].

The impact of incorporating SiO_2 particles on PU membranes is indicated in Fig. 2(a). Obviously, all emerging peaks in the FTIR spectra of SiO_2 are observed in the structure of all nanocomposite membranes. Symmetric and asymmetric vibrations of Si-O-Si bonds appearing at 768 and 1,081 cm^{-1} can serve as a good example. The broadening of the peak at 3,354 cm^{-1} is a characteristic absorption band of O-H stretching of silica into fabricated membranes. By means of these, a harmonious blend of polymer and silica nanoparticles and also the uniform distribution of SiO_2 particles into the polymer matrix show up.

The changes in the absorption region of carbonyl group in polyurethanes are fundamentally examined and depicted in Fig. 2(b). As can be observed, an increase in the amount of SiO_2 content leads to lower intensity of the C=O peak with a wider region. Under this circumstance, the free carbonyl group is relocated to lower frequencies, whereas the urethane-bonded carbonyl group is nearly obliterated. For instance, the peak corresponding to bonded carbonyl in the PU containing 15 wt% of SiO_2 comes to be virtually erased. Absolutely, less formation of hydrogen bonding between the carbonyl and N-H groups of urethane causes the bonded C=O to be broadened and consequently overlapped with the free carbonyl group. The presence of water agent (the O-H band) on the surface of SiO_2 not only induces nanoparticles to interact with the chains of PU, but also interrupts the hydrogen bands in the hard segments in such a way that the N-H groups are considerably reduced in number to be connected to the C=O groups, and thus the intensity of the absorption peak corresponding to the bonded C=O decreases [41]. It means that a higher proportion of nanoparticles have been distributed in the hard phase than the soft phase of matrix. It is crystal clear that this event would be reinforced with increasing the filler amount so the chance of hard phase formation reduces.

1-2. Morphological Study

To study the morphology of all polyurethane membranes, scanning electron microscopy (SEM) was employed. The SEM images of the fabricated samples were taken with a magnification of 50 kX and shown in Fig. 3. The thickness of membranes (cross section area) and the size of nanoparticles were around 100 μm and 30 nm, respectively. It was also detected a densely prepared surface for all polyurethane membranes.

According to Fig. 3, the inclusion of SiO_2 nanoparticles (as an inorganic additive) within the structure of pure PU caused the smooth cross sections of nanocomposite membranes to change their pattern of behavior and lose their unification figures. The cross section images of all nanocomposite membranes exhibit appropriate distribution of filler content in polymeric matrix, which strongly emerged from the existence of good compatibility among polymeric and dispersed phases, as prominently displayed on PETU5 and PETU10 sections. Regarding to this, two key points were achieved. First, a uniform pattern without any structural defects in the matrix of membranes. Second, a good interaction between PU and silica nanoparticles, which effectively prevented the formation of voids at the polymer-particles interface and subsequently resulted in desirable permselectivity.

Although the cross sectional SEM images of the synthesized membranes expressed consistent and proper distribution of silica particles inside the PUs matrices, a loose conglomeration can be seen in some parts of membranes. This agglomeration of style has been frequently reported by researchers at higher loading of different fillers [42-45]. Due to natural affinity of hydroxyl group on the surface of silica nanoparticles, the particles have inherited a marked tendency toward each other, so it might lead to fuse together as one cell. Absolutely, these intermolecular hydrogen bonds would reduce suitable dispersion of nanoparticles within the matrix of polymers, specially for high concentration of nanoparticles and directly affect the performance of nanocomposite membranes.

1-3. Thermal Properties of Membranes

The thermal stability of SiO_2 nanoparticles and PU/SiO_2 nano-

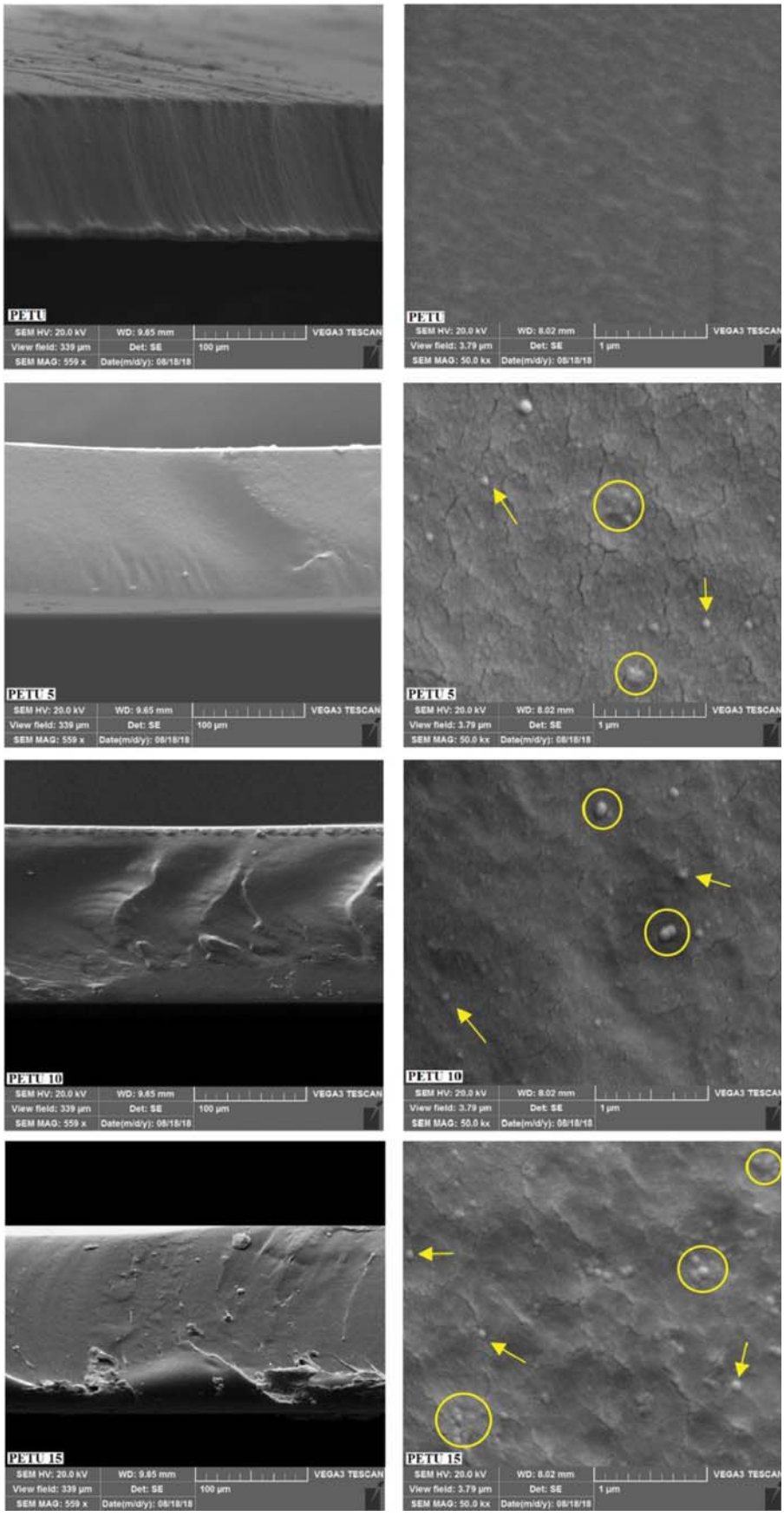

Fig. 3. Cross sectional morphology of PU membranes.

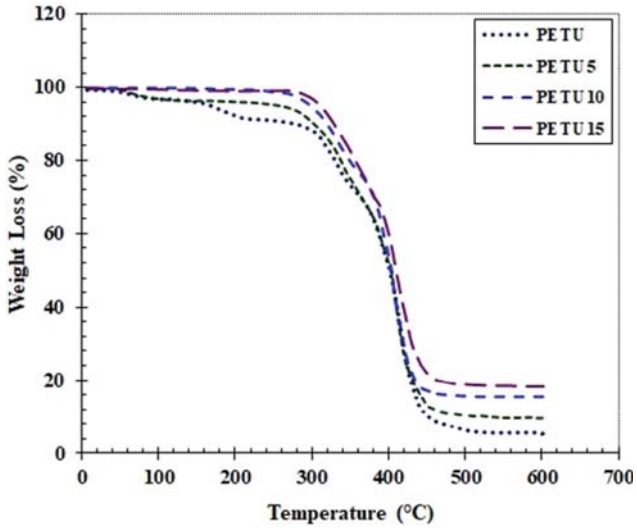

Fig. 4. TGA analysis of neat PU and PU/silica membranes.

composite membranes was appraised using TGA method and the results shown in Fig. 4. As can be seen, the weight loss curve of each sample is composed of three discrete parts: before decomposition (T_d), decomposition and depletion area and finally damping zone, around 200, 290-465 and 465-600 °C, respectively. According to TGA curve, neat PU demonstrates proper thermal stability. From Fig. 4, the neat PU (PETU) allocates the thermal degradation temperature (T_d) of 200 °C, which is related to polymer degradation. Surprisingly, for nanocomposite membranes, the degradation temperature has enormously increased to 290 °C. The enhancement of T_d in fabricated mixed membranes induced by the presence of SiO_2 nanoparticles can be assigned to the high thermal stability of silica nanoparticles which have brilliantly played their

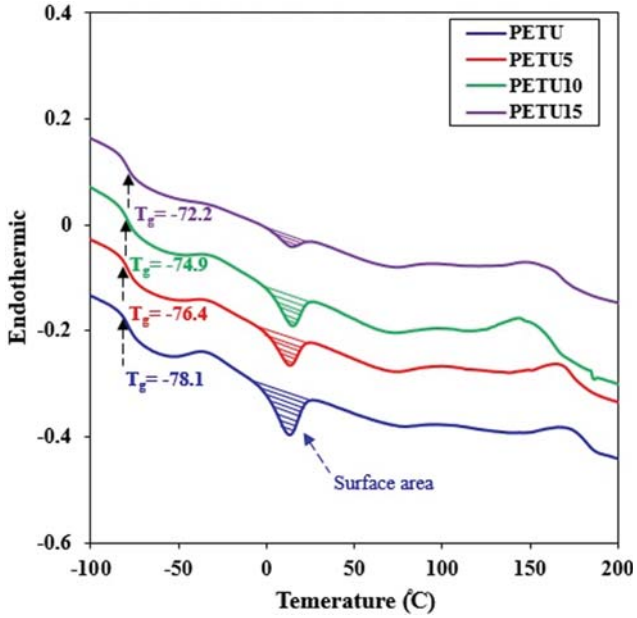

Fig. 5. Heat behavior of nanocomposites of polyurethane/nanoparticles by DSC method.

Table 3. The T_g, melting point and crystallinity degree of each PU membrane

Polymer	T_g (°C)	T_m (°C)	ΔH_f (J/g^{-1})
PETU	−78.1	32.3	36.6
PETU5	−76. 4	34.6	34.1
PETU10	−74.9	36.4	33.4
PETU15	−72.2	38.2	30.2

role as an additive. It can also be taken into account that the strong covalent bond among filler and polymer (SiO_2- PU) enhances the rigidity of chains and ultimately increases the required energy for collapsing the structure of synthesized PU chains. Furthermore, according to Fig. 4, the remaining weight of synthesized membranes is approximately 2, 5, 10 and 15%wt for PETU, PETU5, PETU10 and PETU15, respectively.

DSC curves of the fabricated PUs based on ester are in Fig. 5. In addition, the glass transition temperature (T_g) and the melting temperature of the soft segment are reported in Table 3. Regarding the DSC graph, there are two main crystalline regions for all prepared membranes. First is an endothermic peak between 0-30 °C, which is surely a sign of crystalline area in the soft segment of matrix. The latter has emerged in 140-180 °C, which can be assigned to the formation of crystals inside hard segments. Beyond any doubt, emerging crystalline regions in the hard segments explicitly assert the phase separation of the soft and hard segments in all fabricated samples.

According to Table 3, the T_g of pure PU and PU containing 15 wt% of silica are found −78.1 °C) and −72.2 °C, respectively. As it is obvious, incorporation of SiO_2 nanoparticles into the PU matrix caused the T_g of nanocomposites membranes to go up (ΔT=5.9 °C for the last loading than neat PU). By adding the filler into the polymer structure, an inevitable interaction and chemical cross-linking between the OH groups in the surface of nanosilica and several polar groups of the polymer would occur in such a way that the molecular movement of polymer chain would be severely restricted [46,47] and subsequently the T_g rises. Generally, change in the glass transition temperature of the polymers is assuredly influenced by crystalline area content, the chain stiffness and the inter-chain interactions (with embedded filler content) [48]. Talakesh et al. pronounced that crystallization in soft segments of polymers increases these regions' glass transition temperature [49]. Gheimasi and co-workers declared that increase in the T_g of nanocomposite membranes would arise from its matrix polymer chains, especially those of soft segments, configuration, mobility and rubbery state [35].

To determine crystallinity rate of prepared PU membranes composed of the soft and hard segments, Eq. (4) was used:

$$X_C = \frac{\Delta H_f}{\Delta H_f^0} \tag{4}$$

where X_C is the crystallinity percent of individual membrane, ΔH_f^0 is the heat fusion of the polymer when the membrane is in the state of 100% crystalline structure, and ΔH_f is the heat fusion of the prepared sample counted by integrating the area under the T_m peak detected in the DSC thermograms [50]. Clearly, the crystal-

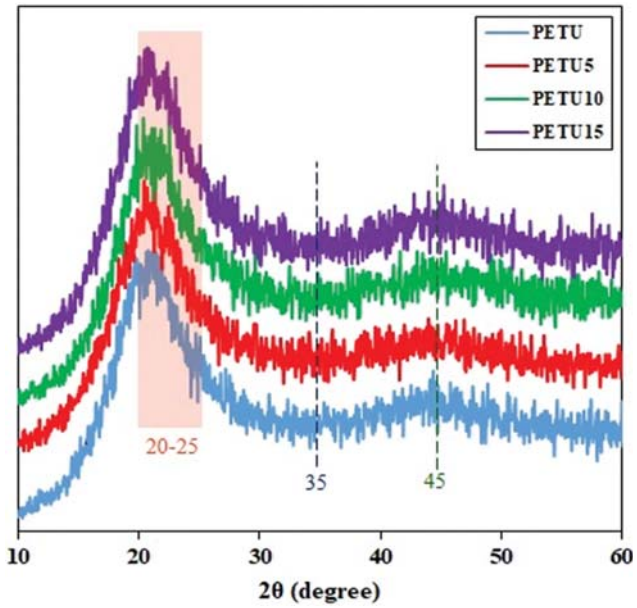

Fig. 6. XRD patterns of etherified and its nanocomposite membranes.

linity degree of polymer would increase when the portion of peaks increases.

The surface areas of membranes in Fig. 5 were also computed by trapezoid method. As it is conspicuous, the crystallinity rate of nanocomposite membrane has reduced in comparison with neat PU and decreased further with more loading of silica content. The amorphous SiO_2 filler causes widespread disruption in the order of chains of the PU; as a result, the crystallinity degree has decreased. Moreover, the small size of nanoparticles causes a uniform dispersion within the matrix of PU and complicates the condition. Previously, several researchers had observed such behavior in which the inclusion of filler content led to a shrinkage of the crystalline regions of polymeric matrix, and consequently the crystallinity degree had decreased [19,34,49,51-53].

1-4. XRD Analysis

The X-ray diffraction of all fabricated membranes is presented in Fig. 6. A broad peak is detected for the pure PU membrane at range of 20-25° assigned to the existence of small crystalline area in the soft and hard segments or the diffraction from large crystals [54]. Furthermore, there are two other crystalline points in 2θ=35° and 45° that indicate the PETU membrane with high crystallinity rate. This is also under the terms of agreement with the appeared peaks in DSC diagram.

As can be seen from Fig. 6, there are no dramatic differences between pure PU and nanocomposites membranes so that all prepared membranes expose relatively the same pattern of behavior. This incident reasonably refers to an even distribution of SiO_2 particles within the matrix of polymer, as previously shown in SEM images. Nonetheless, incorporating silica content into the neat PU intensifies above-mentioned peaks to reduce slightly, which indicates a reduction in crystallinity. Distinctively, disrupting the chain order indispensable for crystallization process is the main reason behind of this [55]. In fact, due to the inclusion of silica nanoparticles, the possibility of the hydrogen bonding formation decreased, and consequently a more amorphous structure with lower crystallinity amount was obtained. This was formerly proved by the FTIR spectra and DSC thermograph.

Table 4. The gas properties of all penetrants used in this research

Penetrant	Critical temp. (°K)	Condensability (°K)	Kinetic dimeter (Å)
CO_2	304.55	195	3.30
O_2	154.581	107	3.46
N_2	126.192	71	3.64

1-5. Gas Permeation Performance

The permeation capability of all three gases through all fabricated membranes was measured over a range of pressures from 6 to 10 bar and of temperatures from 25 to 45 °C. Properties of provided gases are summarized in Table 4. The permeability of polymeric membranes can be described by means of the solution-diffusion mechanism. It reveals that the permeation rate of gas is not only controlled by molecular diffusion, but also it is directly proportional to the dissolution of molecules through polymeric membranes. As is plain, diffusivity is a kinetic factor contingent upon the free space and chain mobility in the polymeric matrix, whereas gas solubility is a thermodynamic factor determined by the chemical and physical interactions between the gas molecule and matrix. Therefore, in the following, we will discuss the influence of adding silica nanoparticle into the matrix of prepared membranes as well as the impacts of increasing feed pressure and temperature on gas transport properties to provide a better insight into molecular mechanism through the membrane.

1-6. Effects of SiO_2 Loading

The permeance rate of synthesized membranes was assessed at different loading of silica articles (5, 10 and 15 wt%) under the variation of input pressure up to 10 bar at ambient condition, 25 °C.

Effect of addition of silica nanoparticles on permeability of CO_2, O_2 and N_2 gases through PU membranes can be deduced from the values listed in Table 5 at pressure of 8 bar. As expected and typical for the permeability of a gas in a rubbery polymer, the amount of permeated gas decreases with increasing filler content, i.e., SiO_2. Furthermore, CO_2 is much more penetrable in that particular PU than O_2 and N_2.

As detected from Table 5, incorporating the silica nanoparticle into the soft and hard segments of PU causes the permeability values of all gases to decrease substantially, i.e., N_2, and this can be generalized to all fabricated membranes in this research. It is a

Table 5. Permeability values of synthesized membranes by adding SiO_2 content at 8 bar and 25 °C

Membrane samples	Permeability (barrer)			Selectivity	
	P_{CO2}	P_{O2}	P_{N2}	$\alpha_{CO2/N2}$	$\alpha_{O2/N2}$
PETU	74.05	7.50	2.74	27.03	2.74
PETU5	72.32	7.31	2.60	27.82	2.81
PETU10	70.51	7.11	2.28	30.93	3.12
PETU15	68.01	6.82	1.93	35.24	3.53

common belief that the inclusion of nanomaterial, i.e., nanoparticles, into the matrix of polymer can improve the performance of membrane by the virtue of changes on the constitutive structure of polymer, as reported in our previous work [3,18,56,57] and also by some researchers [58-60]. Nevertheless, in this study adding filler has decreased the permeation amount of all tested gases. For instance, at the pressure of 8 bar, the permeability value of CO_2 has declined from 74.05 barrer to 68.01 barrer for the pure PU and PU containing 15 wt% of silica, respectively. One possibility might be the restriction of polymeric chain motion arising from the interaction of hydroxyl groups (-OH band) on the surface of SiO_2 with the chains of applied PU. Moreover, it would be realized that impregnating a non-permeable filler, i.e., SiO_2, into the structure of PU polymer, particularly into soft segments, can barricade free spaces and pores and change the passage areas of gas molecules through the matrix in such a way that makes the diffusion path a tortuous one, consequently penetration is reduced [60]. Distinctively, these free volumes in the soft segments, because of their high mobility, would create plenty of spaces for penetrants to diffuse, while incorporation of silica particle acts an obstacle and reduces the accessible free volume and finally leads to permeation of gases decrease.

A precise investigation of the permeability value in Table 5 reveals that the CO_2 gas exhibits markedly better permeation in comparison with other provided gases even at higher filler loading, which can pertain to the smaller kinetic diameter of CO_2. More importantly, the stronger polar interaction, greater condensability and higher critical temperature remarkably intensify the penetration capability of CO_2. These characteristics clearly differentiate CO_2 gas from other gases, such as O_2, N_2, and play major roles in significant enhancement of CO_2 absorption [61-63].

As mentioned, the permeation process of gases into polymeric membranes is considered as an absorption of diffusion and dissolution. In diffusion, the gas molecules are absorbed in the matrix of polymer without chemical reaction, and the amounts of gas permanence are closely connected with the kinematic size of penetrants. According to Table 4, CO_2 which possesses the smallest diameter passes easily over the membranes; thus it allocates higher amount of permeability with respect to O_2 and N_2. But, by adding SiO_2 nanoparticle into the matrix, dissolution mechanism would be powerfully reinforced. As seen in Fig. 7, silica is a hydrophilic nanoparticle that includes polar hydroxyl groups (-OH groups) on its surface which have strong inclination toward other polar groups. Although carbon dioxide is a nonpolar gas, the polarity of the individual C-O bonds in the molecule provides favorable conditions to interact closely with polar groups of other materials. As a result, CO_2 is able to take part in hydrogen bonding and acts as Lewis acid or Lewis base [64,65]. The high polarity of the bonds in the CO_2 molecule allows a strong electron interaction with the highly polar hydroxyl groups in the silica molecules; therefore, this high mutual affinity causes CO_2 absorption to facilitate and consequently CO_2 permeability soars noticeably. To further clarify this claim, regarding Table 4, the permeation rates of CO_2 are 9.87, 9.89, 9.73, 9.97 times than O_2 values and 27.03, 27.82, 30.93, 35.24 times than N_2 amounts within PETU, PETU5, PETU10 and PETU15, respectively.

On the report of Table 5, the permeation trend of all gases shows a reduction in the amount of gases with the addition of filler in a constant temperature, 25 °C. The results show that the sequence of penetration of gases in PU is as follows:

$$CO_2 >> O_2 > N_2$$

Obviously, this order is a general trend for all fabricated membranes, but the permeability amounts of gases would decrease than the former membrane. For example, by increasing the amount of silica particles from 0 wt% to 5, 5 to 10 wt% and 10 to 15 wt% into the matrix of polymer, the permeation value would reduce based on below trend (at 8 bar):

PETU/5: CO_2 (−2.34%)<O_2 (−2.53%)<N_2 (−5.11%)
$\alpha_{(CO2/N2)}$ (2.92%)>$\alpha_{(O2/N2)}$ (2.55%)
PETU5/10: CO_2 (−2.50%)<O_2 (−2.74%)<N_2 (−12.31%)
$\alpha_{(CO2/N2)}$ (11.18%)>$\alpha_{(O2/N2)}$ (11.03%)
PETU10/15: CO_2 (−3.55%)<O_2 (−4.08%)<N_2 (−15.35%)
$\alpha_{(CO2/N2)}$ (13.93%)>$\alpha_{(O2/N2)}$ (13.14%)

As is clear, increasing filler content makes the permeability amounts of all gases decrease, whereas the selectivity values of both gas pairs increase sensibly. Evidently, the reduction trends of both CO_2 and O_2 are approximately close, while N_2 permeability impressively declines. Undoubtedly, the higher reduction rate of N_2 respect to CO_2 and O_2 causes the selectivity of both gas pairs to go decidedly up. However, this increment is slightly greater for CO_2/N_2 com-

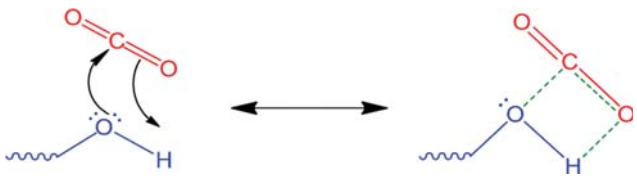

Fig. 7. Polar interaction of CO_2 with hydroxyl group (-OH) on the surface of silica nanoparticle.

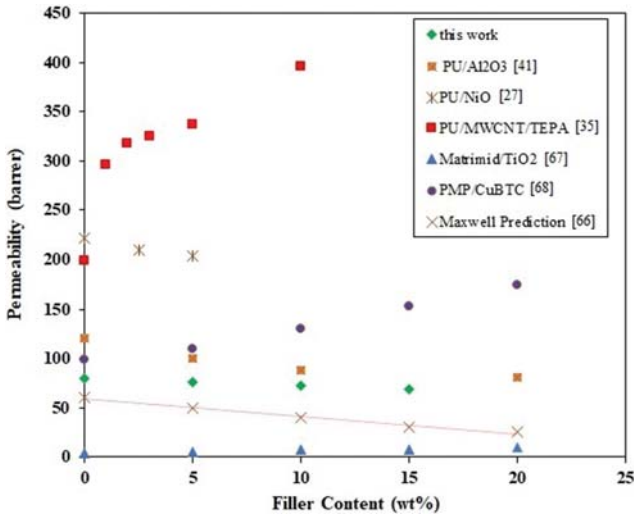

Fig. 8. Comparison of our experimental data and literature data for the CO_2 permeability.

pared to O_2/N_2 gas pairs.

Fig. 8 depicts a comparison of our experimental data and literature data for the permeability of CO_2 in some polymeric membrane impregnated with various types of nanoparticles. Ameri et al. [41] and Molki et al. [27] studied PU with different particles, i.e., Al_2O_3 and NiO, respectively, and found that the incorporation of nanoparticles into the matrix of polymer causes the permeation values of nanocomposite membranes to decrease, as previously predicted by Maxwell [66]. Maxwell believed that the existence of nanoparticles increases tortuosity of the polymer matrix which provides a longer path for diffusion by molecules. Molki et al. stated that the free volume reduction (diffusion) effect overcomes that of favorable CO_2 interaction (solution); as a result, the overall permeability of CO_2 is reduced [27]. Although exact comparison would not be made due to the different pressure and temperature range, our data exhibits similar tendency with their experimental data and Maxwell's prediction. In another study, Gheimasi et al. examined the influence of carbon nanotubes functionalized with tetraethylene pentamine on PU matrix (PU/MWCNT/TEPA). Contrary to expectations, they affirmed that increasing the MWCNT-TEPA loading leads to enhance the penetration of gases within the synthesized membranes since the gas molecules preferentially penetrate through the lower mass transfer resistance region of nanotube structure of MWCNT-TEPA. They also expressed that some interfacial defects such as some voids plus accumulation can provide a tremendous boost for the permeation rates of gases [35]. Nevertheless, this is typical behavior of glassy polymers as reported by Moghadam et al. [67] and Abedini et al. [68], with the latter attributing this augmentation of permeability values to the increase of free volume by loading of MIL 53 particles, which provides a favorable condition for more condensation of CO_2 in membrane matrix. Therefore, type of applied polymers, the methods of fabrication, kind of nanoparticles, operational conditions and even the ambient of laboratory would affect the experiment. All in all, the inclusion of nanoparticles into the structure of polymers might have two contradictory consequences. First, it can improve the penetration of gases caused by widespread disruption in chain packing of matrix, which is commonly observed in the glassy polymers. Second, it acts as a serious impediment, preventing the permeation of gas molecules within the membrane film by increasing diffusion path length [68-71].

1-7. Effect of Feed Gas Pressure

Fig. 9 provides the P-p diagrams (i.e., the permeation value versus the feed pressure) for the systems of gas+PU at different feed gas pressure from 6 to 10 bar at a fixed room temperature, 25 °C. Furthermore, Fig. 10 illustrates the permselectivity of gas pairs with

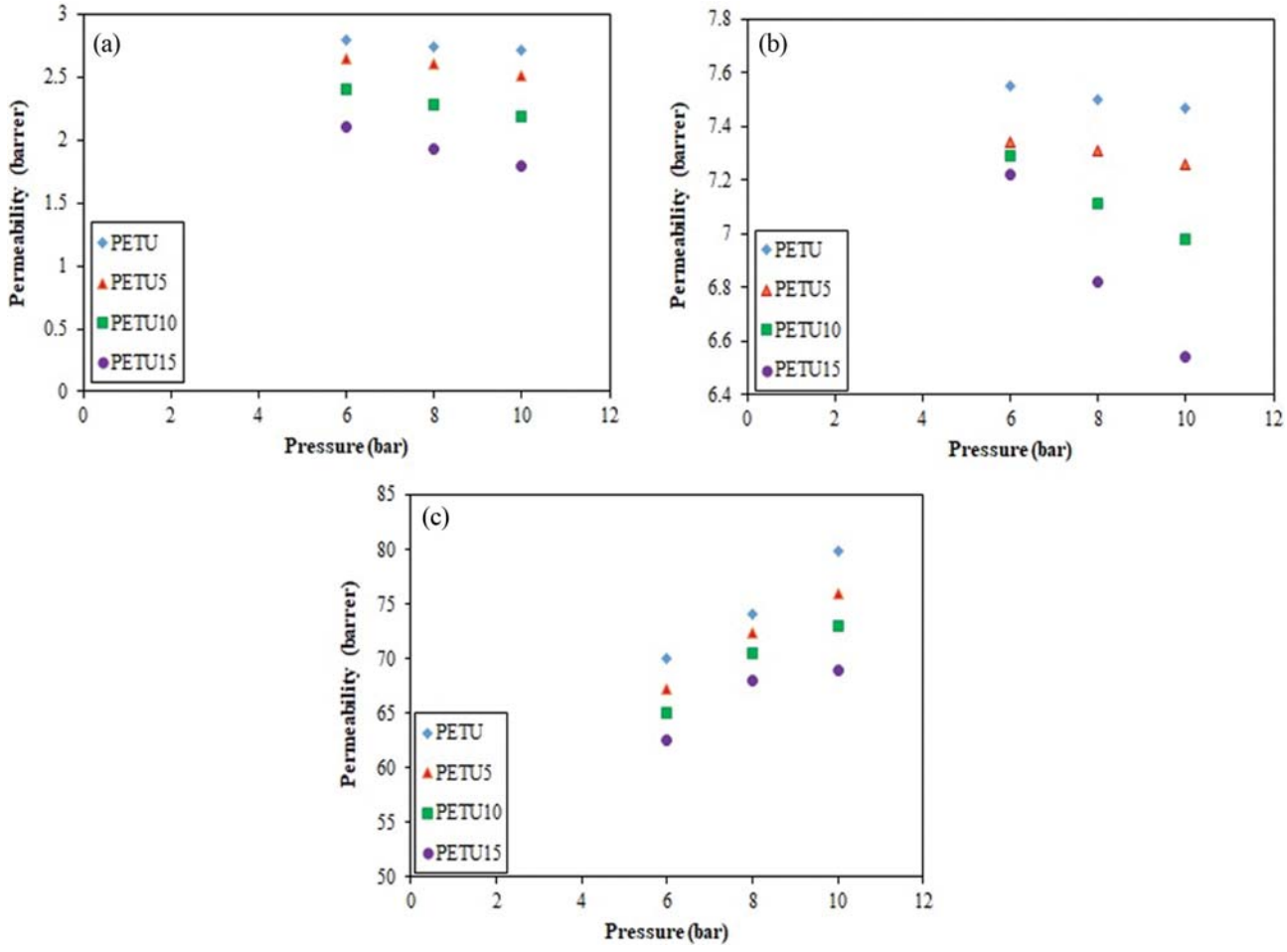

Fig. 9. Effect of feed pressure on the permeability of (a) N_2, (b) O_2 and (c) CO_2 gases.

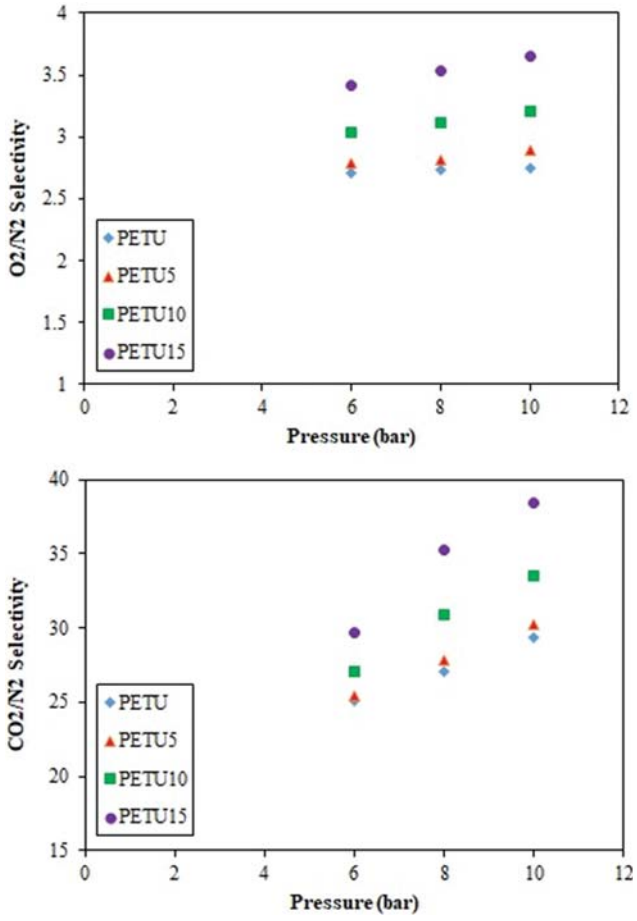

Fig. 10. Effect of pressure on the O_2/N_2 and CO_2/N_2 selectivities for neat PU and PU/silica membranes.

the variation of pressure. Generally, the permeability data reveals that as the feed pressure increases from 6 to 10 bar, the CO_2 permeation is sharply escalated, while the values for O_2 and N_2 are decidedly declined.

As is clear, the magnitude of the gas permeability follows this trend:

$$CO_2 >> O_2 > N_2$$

Utilizing the specifications of the gases from Table 5, the CO_2 gas would show greater permeation value than O_2 and N_2 gases because of its smaller kinematic diameter and higher critical temperature [72,73]. Thus, the smaller the molecular size, the higher the critical temperature and, therefore, the higher the permeation rate through the matrix of polymer. What is more, having high condensability amount results in greater gas solubility, which stimulates the constituents of polymer matrix, i.e., ether groups, to interact with CO_2 and absorb its molecules much more than non-condensable gases such as O_2 and N_2.

As one can see from Fig. 9(a) and (b), the permeation amount of N_2 and O_2 gases would decrease under higher pressure at a constant temperature, 6 to 10 bar at 25 °C, which is in complete contradiction to the value of CO_2 gas (Fig. 9(c)), which ascends steeply with increasing the pressure. Distinctively, increasing the pressure provides a facile permeation conditions for the smaller and condensable gases, i.e., CO_2, in such a way that the molecules can easily pass through the matrix of the polymer. As the case of filler content, adding nanoparticles into the structure of polymer, the pressure might have two plausible hypotheses [3,27]:

I. Increase in the pressure of feed gas increases the gas concentration inside the membrane, in turn, increasing the fractional free volume available into the matrix.

II. The hydrostatic pressure inside the membrane would increase as long as the pressure is high enough; as a result, the free volume contribution would be reduced due to the polymer chain compactness.

Unquestionably, increase of feed gas pressure can radically affect the gas diffusivity as well the solubility of all penetrants through the membrane. As is evident from the data available in Fig. 9(c), the CO_2 values increase with rising pressure so that we firmly believe that the first is the reasonable theory here for CO_2. It means that increase in the volume of condensable gas (gas concentration), i.e., CO_2, results in an increase of the plasticity index owing to the polymer plasticization phenomenon emerging from the strong enough interaction between polar and condensable molecules of CO_2 with the chain packing of polymeric matrix. Besides, the small kinetic size simultaneously assists the molecules of CO_2 to go through easily to show highly significant permeability amount. For instance, the permeation value of CO_2 is 69.93 barrer (at 6 bar), while the corresponding amounts for O_2 and N_2 stand at just 7.55 and 2.79 barrer, respectively. It discloses strikingly that the value of CO_2 is approximately 10 and 25-times the values of O_2 and N_2, respectively.

The other side of coin is a decrease in the permeation rate of gases, definitely, the large and non-condensable molecules, i.e., O_2 and N_2. Failure to interact with the polymer chains and, on the other hand, a large core diameter causes the gases to permeate slightly. Undoubtedly, the incapability to overcome the compression of polymer chains worsens the circumstance and the penetration of gases keeps falling off substantially by increasing the pressure. In case of N_2 gas, the decrement rate is much more than O_2, 3.64 versus 3.46 (Å), respectively; therefore, the gas pair selectivity of O_2/N_2 would increase, whereas the CO_2/N_2 selectivity peaks markedly. To shed light on this point, the trend of changes in permeation values through PETU, for increase of pressure from 6 to 10 bar, is in the order of:

$$CO_2\ (+14.13\%) >> O_2\ (-1.06\%) > N_2\ (-2.51\%)$$

Subsequently, the comparison between selectivities value enhancement is as follows:

$$\alpha_{(CO2/N2)}\ (17.08\%) >> \alpha_{(O2/N2)}\ (1.48\%)$$

According to the FTIR, DSC and XRD results, the phase separation and crystallinity rate decrease, and thus the mixing phase increases in that it would affect the permeation rate of gases in which the contribution of diffusional selectivity of the polymer becomes the predominant feature [49]. Fundamentally, the permeability and permselectivity of penetrants not only are affected by the soft and hard segment chemical structures and contents, but also by the phase separation extent between hard and soft segments in

such materials [74]. Meanwhile, increase of input pressure makes it clearly highlight in such a way that the polymer function would be similar to a glassy polymer. By means of this, the permeance rate of non-condensable gases with large molecular size will lessen and then the polymer selectivity will move positively up. Regarding the above comparison, the increment rate of gas pair selectivity for the condensable gas (CO_2) with respect to the non-condensable gas (O_2) over the largest non-condensable gas (N_2) is relatively 12 times.

From Fig. 9, by inclusion of nanoparticles into the matrix of polymer, the permeation of SiO_2-filled polyurethane is less than pure PU and the former loading of filler. By way of illustration, the permeability values of all penetrants through the all prepared membranes would come with the following ranking:

PETU>PETU5>PETU10>PETU15

For instance, the changes in the permeability and permselectivity of all membranes for provided gases with increasing pressure from 6 to 10 bar, 25 C and different loading of filler are as follows:

PETU: CO_2 (+14.13%)>>O_2 (−1.06%)>N_2 (−2.51%)
α_{PETU}: $\alpha_{(CO2/N2)}$ (17.08%)>$\alpha_{(O2/N2)}$ (1.48%)
PETU5: CO_2 (+13.02%)<O_2 (−1.09%)<N_2 (−4.92%)
PETU/5: CO_2 (−7.86%)<O_2 (−2.83%)<N_2 (−96.02%)
α_{PETU5}: $\alpha_{(CO2/N2)}$ (18.85%)>$\alpha_{(O2/N2)}$ (3.96%)
$\alpha_{PETU/5}$: $\alpha_{(CO2/N2)}$ (10.36%)<$\alpha_{(O2/N2)}$ (167.57%)
PETU10: CO_2 (+12.20%)>>O_2 (−4.25%)<N_2 (−9.17%)
PETU/10: CO_2 (−13.66%)<O_2 (−300.94%)<N_2 (−265.34%)
PETU5/10: CO_2 (−6.30%)<O_2 (−289.91%)<N_2 (−86.38%)
α_{PETU10}: $\alpha_{(CO2/N2)}$ (23.53%)<$\alpha_{(O2/N2)}$ (5.26%)
$\alpha_{PETU/10}$: $\alpha_{(CO2/N2)}$ (37.76%)<$\alpha_{(O2/N2)}$ (255.41%)
$\alpha_{PETU5/10}$: $\alpha_{(CO2/N2)}$ (24.83%)<$\alpha_{(O2/N2)}$ (32.83%)
PETU15: CO_2 (+10.17%)>>O_2 (−9.42%)<N_2 (−15.17%)
PETU/15: CO_2 (−28.03%)<O_2 (−788.68%)<N_2 (−504.38%)
PETU10/15: CO_2 (−16.64%)<O_2 (−121.65%)<N_2 (−65.43%)
α_{PETU15}: $\alpha_{(CO2/N2)}$ (29.86%)>$\alpha_{(O2/N2)}$ (6.73%)
$\alpha_{PETU/15}$: $\alpha_{(CO2/N2)}$ (74.82%)<$\alpha_{(O2/N2)}$ (354.73%)
$\alpha_{PETU5/15}$: $\alpha_{(CO2/N2)}$ (58.41%)<$\alpha_{(O2/N2)}$ (69.95%)
$\alpha_{PETU10/15}$: $\alpha_{(CO2/N2)}$ (26.90%)<$\alpha_{(O2/N2)}$ (27.95%)

This reduction in values for gases can be supported that increasing of feed gas pressure makes the polymer chains be packed closely and, as a result, the free volume of the polymer matrix is reduced [75]. Furthermore, as the free spaces of the matrix of rubbery polymers are much lower compared to glassy polymers, therefore, impregnating nanoparticles into the polymer structure would decrease the contribution of free volume. Assuredly, this circumstance deteriorates in higher amount of loading SiO_2 particles. With reference to the two above-mentioned elements, diffusion of all penetrants is reduced.

1-8. Effect of Feed Gas Temperature

The measured experimental data in the form of PT, where P represents the penetration rate of CO_2, O_2 and N_2 gases permeated within the membrane film at the pressure of 10 bar and T, indicates the operation temperature up to about 45 °C, as tabulated in Tables 6 and 7.

Effect of temperature on permeability of all provided gases through the fabricated membrane can be deduced from the values listed in Tables 6 and 7. As expected, and typical for the permeation of a gas in a polymeric membrane, the amount of penetrated gas increases with rising temperature at a constant pressure. Furthermore, CO_2 is much more permeable in that particular rubbery polymer with respect to O_2 and N_2.

Based on the results obtained in this work, the permeability of all gases (CO_2, O_2 and N_2), expressed in barrer scale, within the PU membranes follows the order: CO_2<O_2<N_2, i.e., the permeability increases with increase in the fractional free volume of matrix of polymer. Talakesh et al. also pointed out this same conclusion [49]. Undoubtedly, by increasing the temperature, the flexibility and dynamic of polymeric chains increase in such a way

Table 6. Permeability and selectivity for CO_2 and N_2 in PETU/ SiO_2 membranes at 10 bar

Samples	Permeability 25 °C		Selectivity	Permeability 35 °C		Selectivity	Permeability 45 °C		Selectivity
	P_{CO2}	P_{N2}	$\alpha_{CO2/N2}$	P_{CO2}	P_{N2}	$\alpha_{CO2/N2}$	P_{CO2}	P_{N2}	$\alpha_{CO2/N2}$
PETU	79.81	2.72	29.34	89.50	3.71	24.12	107.64	4.91	21.92
PETU5	75.98	2.51	30.27	87.16	3.54	24.62	104.59	4.53	23.09
PETU10	73.00	2.18	33.49	82.30	3.11	26.46	99.13	4.13	24.00
PETU15	68.90	1.79	38.49	84.08	2.96	28.41	102.66	4.24	24.21

Table 7. Permeability and selectivity for O_2 and N_2 in PETU/ SiO_2 membranes at 10 bar

Samples	Permeability 25 °C		Selectivity	Permeability 35 °C		Selectivity	Permeability 45 °C		Selectivity
	P_{O2}	P_{N2}	$\alpha_{O2/N2}$	P_{O2}	P_{N2}	$\alpha_{O2/N2}$	P_{O2}	P_{N2}	$\alpha_{O2/N2}$
PETU	7.47	2.72	2.75	9.9	3.71	2.67	11.49	4.91	2.34
PETU5	7.26	2.51	2.89	9.56	3.54	2.70	10.91	4.53	2.41
PETU10	6.98	2.18	3.20	8.58	3.11	2.76	10.24	4.13	2.48
PETU15	6.54	1.79	3.65	8.70	2.96	2.94	10.68	4.24	2.52

that the pattern of movement of the chains would be changed, and subsequently the fraction of free volume into the matrix decidedly increases [27]. It is almost tangible that the penetration rate of large molecules would be facilitated as long as the FV of matrix increases and, in consequence of that, the contribution of the diffusional selectivity would decrease. Accordingly, the gas which allocates larger molecular size, i.e., N_2, has greater permeation rate in comparison with CO_2 which possesses the lowest kinetic diameter. As a result, the permselectivity of gas pairs would dramatically plunge with increase of temperature. For example, the amount of changes in permeation values (Δ_P) through the individual membrane for increasing the temperature in a range of 25 to 45 °C at a constant gas pressure, 10 bar, is as follows:

PETU: N_2 (+80.51)>O_2 (+53.82)>CO_2 (+34.84)
$\alpha_{(O2/N2)}$ (−17.52%)<$\alpha_{(CO2/N2)}$ (−33.85%)
PETU5: N_2 (+73.31)>O_2 (+50.28)>CO_2 (+37.65)
$\alpha_{(O2/N2)}$ (−19.91%)<$\alpha_{(CO2/N2)}$ (−31.10%)
PETU10: N_2 (+89.45)>O_2 (+46.70)>CO_2 (+35.79)
$\alpha_{(O2/N2)}$ (−29.03%)<$\alpha_{(CO2/N2)}$ (−39.54%)
PETU15: N_2 (+136.87)>O_2 (+63.30)>CO_2 (+48.50)
$\alpha_{(O2/N2)}$ (−44.84%)<$\alpha_{(CO2/N2)}$ (−58.98%)

Thus, the increased mutation rate (IMR) by dividing the amount of changes in permeability value of each gas (IMR=Δ_{P1}/Δ_{P2}) is as a sequence of:

PETU: N_2/CO_2=2.311, N_2/O_2=1.460
PETU5: N_2/CO_2=1.947, N_2/O_2=1.458
PETU10: N_2/CO_2=2.499, N_2/O_2=1.915
PETU15: N_2/CO_2=2.822, N_2/O_2=2.162

As illustrated, the permeability value of all gases would sharply climb with increase of temperature, whereas the selectivity of both gas pairs would drastically plummet. As can be noticed, CO_2 gas with the smallest and N_2 gas with the largest molecular size exhibit the lowest and highest penetration amounts through the matrix of prepared membranes with temperature, which makes the selectivity values of CO_2/N_2 fall drastically with respect to the O_2/N_2 amounts. Interestingly, the above results are the complete opposite of the obtained result of increasing feed pressure, in which the permeability of penetrants was reduced, except CO_2, and the selectivity of gas pairs moved up. However, by increasing the temperature and amount of SiO_2 nanoparticles simultaneously, the variation trend of permeability and selectivity is absolutely identical to that of the pressure, drop in overall permeability and advance in overall gas pairs selectivity. For example, at 10 bar and 45 °C, the permeability values of CO_2, O_2 and N_2 in PETU decrease from 107.64, 11.49 and 4.91 barrer to 102.66, 10.68 and 4.24 barrer in PETU15, whereas the gas pairs selectivities of CO_2/N_2 and O_2/N_2 increase from 21.92 and 2.34 to 24.21 and 2.52 for PETU and PETU15, respectively.

As described before, the existence of small crystalline area at range of 20-25° and a narrow and weak peak appearing at 0-30 °C were confirmed by the XRD and DSC analyses, respectively. Also, increasing the operation temperature close to the melting point of such crystals (Table 3) boosts the chain packing of matrix to move easily out of crystal cells in such a way that the crystalline degree of soft segment of matrix decreases and consequently an amorphous Polymer forms [49]. Since the crystal cells are impermeable and act as obstacle in the way of the molecules of penetrants, leaving these cells increases significantly the free spaces required for passing gas through the polymeric film. On the other hand, the formation of crystals into the soft and hard segments would severely restrict the mobility of polymer chains, which leads to a reduction in the diffusion rate of gases. Correspondingly, increasing the temperature would decrease the crystallinity degree of the polymer and provide more spaces for gases to have a facile permeation within the structure of polymer. Briefly, the permeation amount of the penetrants can be raised with the temperature rise factor as a consequence of reducing the degree of crystalline phase to the absolute minimum.

The influence of temperature on the gas permeability is often elucidated using the van't Hoff-Arrhenius equation [76]:

$$P = P_0 \exp\left(\frac{-E_P}{RT}\right) \quad (5)$$

where P_0 [barrer] is the temperature-independent pre-exponential factors, R is the universal gas constant [kJ/mol K], T is the absolute temperature [K], and $-E_P$ is the activation energy of permeation obtained from a logarithmic plot of P versus T^{-1}, [kJ/mol].

Using Eq. (5) and the obtained data in this work, E_P and ΔE_P for all tested gases, i.e., CO_2, O_2 and N_2, were computed and tabulated in Table 8. From Table 8, the obtained ΔE_P values for both gas pairs at pressure of 10 bar are in the order of (in units of kJ/mol):

PETU: O_2/N_2 (10.938)<CO_2/N_2 (15.792)
PETU5: O_2/N_2 (11.066)<CO_2/N_2 (15.869)
PETU10: O_2/N_2 (11.318)<CO_2/N_2 (16.119)
PETU15: O_2/N_2 (11.646)<CO_2/N_2 (16.465)

For gas pairs with higher difference in activation energies (ΔE_P), the dependence of permselectivity on temperature is stronger. Therefore, CO_2/N_2 and O_2/N_2 pairs with the highest and lowest differences in permeation activation energy have the strongest and weakest temperature dependence of permselectivity, respectively.

1-9. Mixed Gas Permeation

The mixed gas permeation property of fabricated membranes was investigated through the gas mixtures of CO_2/N_2 and O_2/N_2 ratios of 50 : 50 v/v. After passing of gas mixtures through the membrane matrix, the impermeable flow was removed, while the permeable gas flow was carried to a GC system to determine the gas composition. The obtained results of gas mixtures, at pressure of 10 bar and temperature of 25 °C, are listed in Tables 9 and 10.

According to Tables 9 and 10, the trend of changes in permea-

Table 8. Permeability activation energy (E_P) for all penetrants at 25 °C and 10 bar

Samples	E_P (kJ/mol)			ΔE_P (kJ/mol)	
	CO_2	O_2	N_2	CO_2/N_2	O_2/N_2
PETU	5.264	10.118	21.056	15.792	10.938
PETU5	5.386	10.189	21.255	15.869	11.066
PETU10	5.485	10.286	21.604	16.119	11.318
PETU15	5.628	10.447	22.093	16.465	11.646

Table 9. Permeability and selectivity for CO_2 and N_2 in PETU/ SiO_2 membranes at 10 bar & 25 °C

Samples	Permeability Pure		Selectivity	Permeability Mixed		Selectivity
	P_{CO2}	P_{N2}	$\alpha_{CO2/N2}$	P_{CO2}	P_{N2}	$\alpha_{CO2/N2}$
PETU	79.81	2.72	29.34	71.19	2.63	27.06
PETU5	75.98	2.51	30.27	69.13	2.46	28.10
PETU10	73.00	2.18	33.49	66.36	2.14	31.00
PETU15	68.90	1.79	38.49	62.56	1.78	35.14

Table 10. Permeability and selectivity for O_2 and N_2 in PETU/ SiO_2 membranes at 10 bar & 25 °C

Samples Gas	Permeability Pure		Selectivity	Permeability Mixed		Selectivity
	P_{O2}	P_{N2}	$\alpha_{O2/N2}$	P_{O2}	P_{N2}	$\alpha_{O2/N2}$
PETU	7.47	2.72	2.75	7.21	2.63	2.74
PETU5	7.26	2.51	2.89	7.08	2.46	2.87
PETU10	6.98	2.18	3.20	6.82	2.14	3.18
PETU15	6.54	1.79	3.65	6.37	1.78	3.57

bility and selectivity values in the mixtures was almost identical with those of pure gas, decrease in permeation, and vice versa increase in gas pair selectivity. For example, the CO_2 permeability in the mixture decreased from 71.19 to 62.56 barrer, while the CO_2/N_2 selectivity was enhanced from 27.06 to 35.14 through PETU and PETU15, respectively. Also, the permeability of all gases and the real selectivities were smaller than the relevant values of pure permeability and ideal selectivity. For instance, the permeation value for CO_2 through PETU decreased from 79.81 to 71.19 barrer, and also its selectivity over N_2 (CO_2/N_2) dropped from 29.34, 27.06, roughly 10% reduction in the values of both indexes.

The reduction of CO_2 permeability and the subsequent decrease in the selectivity values are due largely to the presence of N_2 in the mixture. In fact, the presence of N_2 in the throughput of membranes, which occupy the free volume of the polymer, leads to a reduction in the CO_2 sorption and condensation [4,17]. This scenario is also certainly true for O_2 and N_2 gas mixture. The gaseous mixture results also reveal that CO_2 gas due to its strong tendency to solubility mechanism underwent massive reduction in the rate of permeance, whereas other gases, i.e., O_2 and N_2, illustrated a modest decrement compared to their pure values. Nevertheless, regarding the results presented in Table 9, even though the interaction between the gases in the gas mixture prevents the passing of CO_2 through membrane, the mixed matrix membranes provide an adequate performance for CO_2 capture/separation.

1-10. Performance of Nanocomposite Membranes

In this research, for different structures of the polymer, neat PU (PETU) expressed the highest permeation rate, for instance, up to almost 108 barrer for CO_2 while showed the lowest selectivity for CO_2/N_2, approximately 22. In conflict with that, PU containing 15 wt% (PETU15) delivered a quietly converse performance with the smallest permeability of 62.54 barrer, but the greatest value for

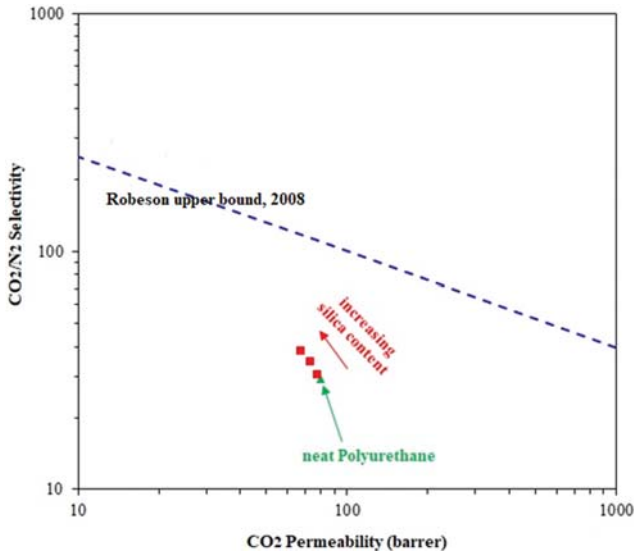

Fig. 11. Comparison of experimental data for CO_2/N_2 separation with Robeson' upper bound.

CO_2/N_2, nearly 39. As can be noticed, increase in the permeation rate makes the selectivity value of gas pair to decline decidedly. Thus, regarding this serious challenge between the permeability and selectivity, a strict criterion is vital to be defined based on these two key parameters for practical purposes and commercialization [77-79]. Our experimental results from the synthesized PU/SiO_2 membranes were compared with the upper bound limit of Robeson (Robeson's 2008) in Fig. 11. As depicted in the figure, the CO_2/N_2 separation results of the fabricated membranes show a slight inclination to approach to Robeson's line by impregnation of membranes matrix with SiO_2 nanoparticles. This acceptable behavior recommends better separation performance for the ideal selectivity of CO_2/N_2 as well as O_2/N_2 gas pair, whereas the permeability values decrease in the nanocomposite membranes. Nevertheless, some other attempts are reasonably required to enhance the ratio of permeation and selectivity of nanocomposite membranes to overcome this limit, which is under feasibility study.

Table 11 offers a comparison of the performance of various membranes filled with particles for the experimental data obtained in this work and literature data. As can be detected, the penetration of gases and also the selectivity of pair gases have been affected by the operational conditions, i.e., T and P, as well as type of filler content. According to Table 11, the mixed matrix membranes of PU express suitable permeability. Moreover, the synthesized membranes based PU almost demonstrate more selectivity with respect to other polymers. These outcomes firmly corroborate that PU with new chain extender, MOCA, would be able to act as a versatile polymer with high performance for pragmatic applications in various processes of industry, such as gas separation.

CONCLUSION

PU/SiO_2 nanocomposite membranes were prepared and tested under different operation conditions and loading of filler, and their various properties were characterized and discussed. The main

Table 11. A comparison between several selected MMMs and this work for CO_2/N_2 separation

Polymer	Filler	Loading (wt%)	Operating conditions		P_{CO2}	P_{N2}	$\alpha_{CO2/N2}$	Ref.
			T (°C)	P (bar)				
PMP	Al_2O_3	10	25	4	185.80	2.71	68.58	[3]
PSF	TiO_2	15	35	10	13	1.11	14.94	[45]
Matrimid	SiO_2	15	35	10	11.1	0.79	14.14	[45]
PPO_{dm}	SiO_2	9	25	0.68	48.40	3.30	14.70	[80]
PU (BDO)	NiO	5	30	5	131	3.51	37.32	[27]
PU (BDO)	---	---	25	6	96.83	3.12	31.04	[49]
PU (BDO)	TiO_2	30	25	10	98	2.80	35	[60]
PUU [PPG2700] (EDA)	---	---	35	5	190	11	17.27	[74]
PUU [Terathane: PEG] (EDA)	---	---	35	5	150	7.2	20.83	[74]
PU (IPDI)	---	---	25	4	61.9	2	30.95	[81]
PETU15(MOCA)	SiO_2	15	25	10	68.90	1.79	38.49	This work

conclusions are as follows:

I. The presence of SiO_2 nanoparticles was confirmed by FRIT analysis due to changes in absorption bands and their intensity, such as the bonded carbonyl group which eventually overlapped with the free carbonyl group. Also, the smooth cross section structure of nanocomposite membranes lost its assimilation pattern owing to incorporating silica into the matrix of polymer.

II. The thermal stability of nanocomposite membranes dramatically increased because of the high thermal stability of SiO_2 nanoparticles. The glass transition temperature of polymers increased from −78.1 °C to −72.2 °C for PETU and PETU15, respectively, due to increase in phase interference or decrease in phase separation. Further, the XRD results indicated small crystalline regions in soft and hard segments in the matrix of PUs membranes.

III. The CO_2, O_2 and N_2 permeability decreased from 74.05, 7.50 and 2.74 barrer in pure PU to 68.01, 6.82 and 1.93 barrer in PU containing 15 wt% SiO_2 nanoparticles. Undoubtedly, this decrement in values could be assigned to longer diffusion path and also decrease in free volume as well as the agglomeration of nanoparticles, which reduced the sorption and diffusion of penetrants within the matrix of fabricated membranes.

IV. Because of interaction with polymer chains, the CO_2 permeation went decidedly up with the pressure, whereas a reduction in permeance values for O_2 and N_2 occurred through the membranes by increasing the feed gas pressure. Nonetheless, the selectivity values of gas pairs, CO_2/N_2 and O_2/N_2, increased positively.

V. By increasing the feed gas temperature, the permeability of all penetrants rose sharply, which was mainly due to the increase in the fractional free volume of matrix. However, the permselectivity of both gas pairs declined dramatically. The selectivity value of CO_2/N_2 decreased from 29.34 at 25 °C and 10 bar to 21.92 at 45 °C in PETU, while the corresponding amount at 45 °C in PETU15 was about 24.21.

Finally, regarding the obtained results, it must be pointed out that PU with new chain extender named MOCA is a viable alternative when aiming at a highly selective polymer for CO_2/N_2 separation. Although this novel nanocomposite membrane is attractive in its acceptable performance, the capacities of this new polymer for the gas separation process have to be assessed by future research with applying more selective nanoparticles and crosslinking and blending with other polymer. In future study, we will focus on new approaches to obtain more favorable results for process of industrialization.

ABBREVIATIONS

PU : polyurethane
PUU : polyurethane-urea
PETU : polyetherurethane
PTMG : polytetramethylene glycol
DI : diisocyanates
HDI : hexamethylene diisocyanate
MOCA : 4,4-methylenebis(2-chloroaniline)
DBTDL : dibutyltin dilaurate
NMP : N-methyl-2-pyrrolidone
PIMs : polymers of intrinsic microporosity
PMP/TPX : poly (4-methyl-1-pentene)
PPO : poly (2,6-dimethyl-1,4-phenylene oxide)
PA : polyamide
PPG : ploy (propylene glycol)
Terathane : poly (tetramethylene ether glycol)
PEG : ploy (ethylene glycol)
BDO : 1,4-butandiol
IPDI : isophorone diisocyanate
EDA : ethylene diamine
OCDA : octanediamine
SGWF : short glass wool fiber
TEPA : tetraethylene pentamine
TiO_2 : titanium oxide
Al_2O_3 : aluminium oxide (Alumina)
SiO_2 : silicon dioxide (Silica)
NiO : nickel oxide
FV : free volume
FFV : fractional free volume

REFERENCES

1. M. H. Nematollahi and P. J. Carvalho, *Curr. Opin. Green Sustain.*

Chem., **18**, 25 (2019).
2. C. Y. Feng, K. C. Khulbe, T. Matsuura and A. F. Ismail, *Sep. Purif. Technol.*, **111**, 43 (2013).
3. M. H. Nematollahi, A. H. Saeedi Dehaghani and R. Abedini, *Korean J. Chem. Eng.*, **33**, 657 (2016).
4. M. Mozafari, R. Abedini and A. Rahimpour, *J. Mater. Chem. A*., **6**, 12380 (2018).
5. T. C. Merkel, B. D. Freeman, R. J. Spontak, Z. He, I. Pinnau, P. Meakin and A. J. Hill, *Chem. Mater.*, **15**, 109 (2003).
6. L. Shao, J. Samseth and M. B. Hägg, *J. Membr. Sci*., **326**, 285 (2009).
7. L. Olivieri, S. Ligi, M. G. De Angelis, G. Cucca and A. Pettinau, *Ind. Eng. Chem. Res.*, **54**, 11199 (2015).
8. R. Abedini, A. Mosayebi and M. Mokhtari, *Process Saf. Environ. Prot.*, **114**, 229 (2018).
9. T. C. Merkel, Z. He, I. Pinnau, B. D. Freeman, R. J. Spontak, P. Meakin and A. J. Hill, *Macromolecules*, **36**, 8406 (2003).
10. Y. Okamoto, Q. Du, K. Koike, F. Mikeš, T. C. Merkel, Zh. He, H. Zhang and Y. Koike, *Polym. Adv. Technol.*, **27**, 33 (2016).
11. B. J. Sundell, J. A. Lawrence, D. J. Harrigan, J. T. Vaughn, T. S. Pilyugina and D. R. Smith, *RSC Adv.*, **6**, 51619 (2016).
12. N Belov, R. Nikiforov, L. Starannikova, K. R. Gmernicki, C. R. Maroon, B. K. Long, V. Shantarovich and Y. Yampolskii, *Eur. Polym. J.*, **93**, 602 (2017).
13. M. L. Chu, Y. C. Xiao and T. S. Chung, *J. Membr. Sci.*, **415-416**, 375 (2012).
14. Y. Rogan, R. Malpass-Evans, M. Carta, M. Lee, J. C. Jansen, P. Bernardo, G. Clarizia, E. Tocci, K. Friess, M Lanc and N. B. McKeown, *J. Mater. Chem. A.*, **2**, 4874 (2014).
15. B. S. Ghanem, R. Swaidan, E. Litwiller and I. Pinnau, *Adv. Mater.*, **26**, 3688 (2014).
16. R. Swaidan, B. S. Ghanem, E. Litwiller and I. Pinnau, *J. Membr. Sci.*, **457**, 95 (2014).
17. R. Abedini, M. R. Omidkhah and F. Dorosti, *RSC Adv.*, **4**, 36522 (2014).
18. M. H. Nematollahi, A. H. Saeedi Dehaghani, V. Pirouzfar and E. Akhondi, *Macromol. Res.*, **24**, 782 (2016).
19. R. S. Murali, S. Sridhar, T. Sankarshana and Y. V. L. Ravikumar, *Ind. Eng. Chem. Res.*, **49**, 6530 (2010).
20. M. A. Semsarzadeh and B. Ghalei, *J. Membr. Sci.*, **432**, 115 (2013).
21. S. Gh. Lovineh, M. Asghari and G. Khanbabaei, *Appl. Surf. Sci.*, **318**, 176 (2014).
22. J. T. Vaughn and W. J. Koros, *J. Membr. Sci*., **465**, 107 (2014).
23. V. Mozaffari, M. Sadeghi, A. Fakhar, G. Khanbabaei and A. F. Ismail, *Sep. Purif. Technol.*, **185**, 202 (2017).
24. E. N. Guseva and V. V. Zuev, *Fuller. Nanotub. Car.*, **24**, 474 (2016).
25. D. K. Chattopadhyay and K. V. S. N. Raju, *Prog. Polym. Sci*., **32**, 352 (2007).
26. M. A. Semsarzadeh, B. Ghalei, M. Fardi, M. Esmaeeli and E. Vakili, *Korean J. Chem. Eng*., **31**, 841 (2014).
27. B. Molki, W. Aframehr, R. Bagheri and J. Salimi, *J. Membr. Sci.*, **549**, 588 (2018).
28. J. N. Gavgani, H. Adelnia and M. M. Gudarzi, *J. Mater. Sci*., **49**, 243 (2007).
29. M. Joshi, B. Adak and B. S. Butola, *Prog. Mater. Sci.*, **97**, 230 (2007).
30. H. R. Amedi and M. Aghajani, *J. Nat. Gas Sci. Eng.*, **35**, 695 (2007).
31. F. Aghili, A. A. Ghoreyshi, A. Rahimpour and M. Rahimnejad, *Process Saf. Environ. Prot.*, **107**, 528 (2007).
32. N. Azizi, T. Mohammadi and R. M. Behbahani, *J. Nat. Gas Sci. Eng.*, **37**, 39 (2007).
33. Sh. Shi, D. Shen and T. X. Y. Zhang, *Compos. Sci. Technol.*, **164**, 17 (2007).
34. H. T. Afarani, M. Sadeghi, A. Moheb and E. N. Esfahani, *Chin. J. Chem. Eng.*, **27**, 110 (2019).
35. K. M. Gheimasi, O. Bakhtiari and M. Ahmadi, *Chem. Eng. Res. Des.*, **133**, 222 (2007).
36. M. B. Karimi and Sh. Hassanajili, *J. Membr. Sci.*, **543**, 4048 (2007).
37. M. Sadeghi, M. M Talakesh, B. Ghaeli and MR. Shafiei, *J. Membr. Sci.*, **427**, 21 (2013).
38. A. Beganskiene, V. Sirutkaitis, M. Kurtinaitiene, R. Juskenas and A. Kareiva, *Mater. Sci.*, **10**, 287 (2007).
39. E. Yılgor, I. Yılgor and E. Yurtsever, *Polymer*, **43**, 6551 (2007).
40. L. Bistricic, G. Baranovic, M. Leskovac and E. G. Bajsic, *Eur. Polym. J.*, **46**, 1975 (2007).
41. E. Ameri, M. Sadeghi, N. Zarei and A. Pournaghshband, *J. Membr. Sci.*, **479**, 11 (2007).
42. Sh. Hassanajili, E. Masoudi, Gh. Karimi and M. Khademi, *Sep. Purif. Technol.*, **116**, 1 (2007).
43. Sh. Hassanajili, M. Khademi and P. Keshavarz, *J. Membr. Sci.*, **453**, 369 (2007).
44. F. Dorosti, M. R. Omidkhah and R. Abedini, *Chem. Eng. Res. Des.*, **92**, 2439 (2007).
45. M. Jamshidi, V. Pirouzfar, R. Abedini and M. Z. Pedram, *Korean J. Chem. Eng.*, **34**, 829 (2007).
46. C. J. Orme, M. K. Harrup, T. A. Luther, R. P. Lash, K. S. Houston, D. H. Weinkauf and F. F. Stewart, *J. Membr. Sci.*, **186**, 249 (2007).
47. R. Gharibi, A. Ghadimi, H. Yeganeh, B. Sadatnia and M. Ghareda-aghi, *J. Membr. Sci.*, **548**, 572 (2018).
48. C. Zhang, P. Li and B. Cao, *J. Membr. Sci*., **530**, 176 (2017).
49. M. M. Talakesh, M. Sadeghi, M. Pourafshari Chenar and A. Khosravi, *J. Membr. Sci.*, **415-416**, 469 (2012).
50. J. H. Lee, C. H. Park, J. P. Jung, J. H. Kim and J. H. Kim, *Chem. Eng. J.*, **334**, 939 (2018).
51. T. Zhou, L. Luo, S. Hu, S, Wang, R. Zhang, H. Wu, Z. Jiang, B. Wang and J. Yang, *J. Membr. Sci.*, **489**, 1 (2015).
52. H. Rabiee, Sh. Meshkat, M. Soltanie, S. A. Mousavi and A. Ghadimi, *J. Ind. Eng. Chem*., **27**, 223 (2015).
53. Z. Aghaei, L. Naji, V. Hadadi Asl, Gh. Khanbabae and F. Dezhagah, *Sep. Purif. Technol.*, **199**, 47 (2018).
54. M. Sadeghi, M. A. Semsarzadeh, M. Barikani and B. Ghalei, *J. Membr. Sci.*, **354**, 40 (2010).
55. S. Mondal and J. L. Hu, *J. Membr. Sci.*, **274**, 219 (2006).
56. H. Hosseinzadeh Beiragh, M. R. Omidkhah, R. Abedini, T. Khosravi and S. Pakseresht, *Asia-Pacific J. Chem. Eng.*, **11**, 522 (2016).
57. E. Nezhadmoghadam, M. Pourafshari Chenar, M. R. Omidkhah, A. Nezhadmoghadam and R. Abedini, *Korean J. Chem. Eng.*, **35**, 526 (2018).
58. J. Ahn, W. J. Chung, I. Pinnau and M. D. Guiver, *J. Membr. Sci.*, **314**, 123 (2008).
59. I. Tirouni, M. Sadeghi and M. Pakizeh, *Sep. Purif. Technol.*, **141**, 394 (2015).
60. M. Sadeghi, H. T. Afarani and Z. Tarashi, *Korean J. Chem. Eng.*, **32**, 97 (2015).

61. L. Abdellah, B. Boutevin, F. Guida-Pietrasanta and M. Smaihi, *J. Membr. Sci.*, **217**, 295 (2003).
62. H. Zhou, Y. Chen, H. Fan, H. Shi, Z. Luo and B. Shi, *J. Membr. Sci.*, **318**, 71 (2008).
63. Sh. Saedi, S. S. Madaeni, K. Hssanzadeh, A. A. Shamsabadi and S. Laki, *J. Ind. Eng. Chem.*, **20**, 1916 (2014).
64. O. Aschenbrenner and P. Styring, *Energy Environ. Sci.*, **3**, 1106 (2010).
65. A. Shamiri, M. S. Shafeeyan, H. C. Tee, C. Y. Leo, M. K. Aroua and N. Aghamohammadi, *J. Nat. Gas Sci. Eng.*, **35**, 605 (2016).
66. C. Maxwell, Treatise on Electricity and Magnetism, Oxford Univ. Press, London (1873).
67. F. Moghadam, M. R. Omidkhah, E. Vasheghani-Farahani, M. Z. Pedram and F. Dorosti, *Sep. Purif. Technol.*, **77**, 128 (2011).
68. R. Abedini, M. R. Omidkhah and F. Dorosti, *Int. J. Hydrogen Energy*, **39**, 7897 (2014).
69. H. Cong, M. Rados, B. F. Towler and Y. Shen, *Sep. Purif. Technol.*, **55**, 281 (2007).
70. M. Aroon, A. Ismail, T. Matsuura and M. Montazer-Rahmati, *Sep. Purif. Technol.*, **75**, 229 (2010).
71. S. A. Hashemifard, A. F. Ismail and T. Matsuura, *Chem. Eng. J.*, **170**, 316 (2011).
72. A. Bos, I. G. M. PuÈnt, M. Wessling and H. Strathmann, *J. Membr. Sci.*, **155**, 67 (1999).
73. M. A. Semsarzadeh, M. Sadeghi, M. Barikani and H. Moadel, *Iran. Polym. J.*, **16**, 819 (2007).
74. H. Li, B. D. Freeman and O. M. Ekiner, *J. Membr. Sci.*, **369**, 49 (2011).
75. S. A. Stern and S. M. Fang, *J. Polym. Sci.*, **10**, 201 (1972).
76. M. Sadrzadeh, K. Shahidi and T. Mohammadi, *J Membr. Sci.*, **342**, 327 (2009).
77. L. M. Robeson, *J. Membr. Sci.*, **62**, 165 (1991).
78. S. Rafiq, Z. Man, S. Maitra, A. Maulud, F. Ahmad and N. Muhammad, *Korean J. Chem. Eng.*, **28**, 2050 (2011).
79. M. A. Semsarzadeh, B. Ghalei, M. Fardi, M. Esmaeeli and E. Vakili, *Korean J. Chem. Eng.*, **31**, 841 (2014).
80. H. Cong, X. Hu, M. Radosz and Y. Shen, *Ind. Eng. Chem. Res.*, **46**, 2567 (2007).
81. A. P. Isfahani, B. Ghalei, R. Bagheri, Y. Kinoshita and H. Kitagawa, *J. Membr. Sci.*, **513**, 58 (2007).